Physics Letters A 530 (2025) 130133

Contents lists available at ScienceDirect

Physics Letters A

journal homepage: www.elsevier.com/locate/pla

Letter

Elastic deformation of symmetrical conducting materials in electric field

Fuqian Yang

Materials Program, Department of Chemical and Materials Engineering, University of Kentucky, Lexington, KY 40506, United States

ARTICLE INFO

Communicated By Lilia Woods

Keywords:
Electric stress
Core-shell structure
Deformation
Stress

ABSTRACT

In this work, we study field-induced stress in cylindrical and spherical core-shell structures with linear elasticity. The solid conducting core, which carries a net electric charge, experiences hydrostatic tensile stress for spherical structure and tensile stress in radial, axial and azimuth directions for cylindrical structure. The conducting shell is subjected to tensile stress in the radial direction and compressive stress in the azimuth direction for both the spherical and cylindrical structures. The radial tensile stress can cause the formation and propagation of cracks. For a section of the shell with the planar faces parallel to symmetrical axis, the field-induced force on the section is repulsive when the distance between the symmetrical axis and the section of the shell is larger than the critical distance.

Introduction

The interaction between electric charge and electric field can cause the separation of the gravity center of electron from the corresponding one of positive charge (ion), resulting in changes in the microstructure of materials. The studies of field-induced changes in the microstructures of materials have led to the finding of field-induced polarization [1–3], piezoelectricity [2,4,5], electrostriction [6–9], and so forth, and opened new frontiers in the fields of smart devices and systems. On the other hand, there have been extensive studies on field-induced shape changes of liquid droplets as well as field-induced fluid flow, which is considered as a branch of fluid dynamics under electric field and referred to electrohydrodynamics [10–13]. In the heart of the field-induced changes in microstructures and fluid flow are the electric force on electric charge/dipole and/or the electric stress generated by electric field.

In contrast to the studies of piezoelectricity, electrostriction, and electrohydrodynamics, there are few works on field-induced deformation of electric conductors. Landau et al. [14] in the book “Electrodynamics of Continuous Media” briefly discussed the changes in the volume and shape of a conducting sphere in a uniform electric field. Hansen et al. [15] analyzed the elastic deformation of a semi-infinite metallic material due to electrostatic pressure induced by a voltage bias. Yang and Song [16,17] analyzed surface instability of elastic conducting films and semi-infinite conducting materials in electric field with the contribution of field-induced deformation. Huang [18] studied surface instability of an elastic conducting film in an electric field without the field-induced deformation.

Recently, field-assisted forming and machining of metallic materials [19–22] and field-assisted energy storage [23–26] have attracted great attention. One of concerns in the applications of these processes is the structural integrity of materials and devices in electric field, i.e., field-induced deformation and structural changes, even though studies have been conducted on electroplasticity of metallic materials with the passing of electric current [27–34]. The field-induced deformation of mechanical structures and systems can lead to the failure and/or malfunction of the structures and systems. For example, applying high-voltage electric pulses led to the roughening of stainless-steel surface placed in a 154 mM NaCl solution [35] and the dispersion of small lead particles in grain boundaries of a Cu–Zn alloy [36]. Liu et al. [37] reported that the mechanical behavior of CrMnFeCoNi high-entropy-alloy processed by field-assisted machining with ion beam is dependent on the ions (Xe^+ and Ga^+) used in the machining. Electrochemical cycling can lead to structural damage/degradation of electrode materials, such as Si [38,39].

Currently, field-assisted processing with ion beam has been used to machine inner surface of metallic tube structures [22]. Core-shell structures, such as spherical and cylindrical core-shells [40,41], have been used to accommodate cycling-induced swelling of electrode materials, mitigate structural damage of electrode materials induced by electromotive stress and diffusion-induced stress, and prolong the lifespan of metal-ion batteries [42–44]. An et al. [40] used micro-spherical Si/C core-shell structures, which consist of Si nanoparticle as solid core and a thin C as shell, as anode materials of lithium-ion batteries, which retained 81.4% of the initial capacity after 1200 cycles. Liu et al. [41] demonstrated that lithium-ion batteries with core-shell Bi@C nanowires as anode materials exhibited long-cyclic life. These studies point to the

---

E-mail address: fuqian.yang@uky.edu.

https://doi.org/10.1016/j.physleta.2024.130133
Received 23 September 2024; Received in revised form 25 November 2024; Accepted 28 November 2024

effectiveness of core-shell structures in improving the structural integrity of lithium-ion batteries. However, few have focused on field-induced deformation of core-shell structures, which is of practical importance to understand the deformation of mechanical structures in an electric field.

The purpose of this work is targeted at the elastic deformation of symmetrical structures consisting of a conducting solid core and a conducting shell, i.e., the cylindrical core-shell and spherical core-shell structures shown schematically in Fig. 1, with the conducting core carrying electric charge. The deformation and stress fields in the conducting core and conducting shell were obtained. For the conducting shell, the field effect on the resultant force onto a section of the shell with planar faces parallel to axisymmetric axis was discussed.

Mathematical formulations

For a conducting material, the electric field intensity, **E**, at the surface of the conducting material with ρ_s as the surface charge density, as shown in Fig. 1a, is

$$\mathbf{E} = \frac{\rho_s}{\varepsilon_0}\mathbf{n}. \tag{1}$$

Here, ε_0 is the dielectric constant of the air, and **n** is the unit outward normal on the surface. The electric field introduces normal stress, $\boldsymbol{\sigma}_n$, on the surface as

$$\boldsymbol{\sigma}_n = \frac{1}{2}\rho_s\mathbf{E}. \tag{2}$$

The normal stress leads to the deformation of the conducting material. Assume that the conducting material is isotropic and homogeneous. For elastic deformation with small strain, the theory of linear elasticity is used. The constitutive relations are

$$\boldsymbol{\varepsilon} = \frac{1}{E}[(1+\nu)\boldsymbol{\sigma} - \nu\,\mathrm{tr}(\boldsymbol{\sigma})\mathbf{I}]. \tag{3}$$

The equilibrium equations describing the elastic deformation of the conducting material without body force can be formulated as

$$\nabla^2\mathbf{u} + \frac{1}{1-2\nu}\nabla \in = 0. \tag{4}$$

The dilatation, $\in = \nabla\bullet\mathbf{u}$, satisfies the Laplace equation as

$$\nabla^2 \in = 0. \tag{5}$$

Here, $\boldsymbol{\varepsilon}$ and $\boldsymbol{\sigma}$ are the strain and stress tensors, respectively, **u** is the displacement vector, and E and ν are the Young's modulus and Poisson's ratio of the conducting material, respectively. The boundary condition is

$$\boldsymbol{\sigma}\cdot\mathbf{n} = \boldsymbol{\sigma}_n. \tag{6}$$

Eqs. (2)–(6) form the basis to analyze the field-induced deformation of conducting material.

Deformation and stress fields

Using Eqs. (2)–(6), we analyze the field-induced deformation in two configurations, as shown in Fig. 1b-c. The first one consists of a cylindrical conducting solid core and a cylindrical conducting shell, and the second one consists of a spherical conducting solid core and a spherical conducting shell. The solid core carries electric charge, which uniformly distributes on the surface.

A cylindrical conducting solid core enclosed with a co-axial cylindrical conducting shell

For the structure of a cylindrical conducting solid core with a co-axial cylindrical conducting shell, the cylindrical solid core carries electric charge, which induces opposite electric charge on the inner surface of the co-axial cylindrical conducting shell and electric charge of the same sign on the outer surface of the co-axial cylindrical conducting shell. Let Q be electric charges per unit length carried by the cylindrical solid core. Provided that electric charges are uniformly distributed over individual surfaces, the charge densities on the surfaces are

$$\rho_a = \frac{Q}{2\pi a},\ \rho_b = -\frac{Q}{2\pi b} \text{ and } \rho_c = \frac{Q}{2\pi c} \tag{7}$$

for the surfaces with the radii of a, b, and c ($a < b < c$), respectively. Here, a is associated with the surface of the cylindrical solid core; b and c are associated with the inner and outer surfaces of the cylindrical conducting shell, respectively. Using Eq. (1), the electric field intensities on individual surfaces are found to be

$$\mathbf{E}_a = \frac{Q}{2\pi\varepsilon_0}\frac{1}{a}\mathbf{e}_r,\ \mathbf{E}_b = \frac{Q}{2\pi\varepsilon_0}\frac{1}{b}\mathbf{e}_r \text{ and } \mathbf{E}_c = \frac{Q}{2\pi\varepsilon_0}\frac{1}{c}\mathbf{e}_r \tag{8}$$

with $\mathbf{e}_r$ as the radial direction. According to Eq. (2), the normal stresses on the corresponding surfaces are

$$\sigma_n^{(a)} = \frac{1}{2\varepsilon_0}\left(\frac{Q}{2\pi a}\right)^2,\ \sigma_n^{(b)} = \frac{1}{2\varepsilon_0}\left(\frac{Q}{2\pi b}\right)^2 \text{ and } \sigma_n^{(c)} = \frac{1}{2\varepsilon_0}\left(\frac{Q}{2\pi c}\right)^2 \tag{9}$$

Here, the superscripts and subscripts of a, b, and c represent the surfaces with the radii of a, b, and c, respectively. It is evident that all the surfaces are subjected to tensile normal stress.

With the characteristics of axisymmetric symmetry, Eqs. (4)-(5) and the equation of $\in = \nabla\bullet\mathbf{u}$ are simplified as

$$\frac{1}{r}\frac{\partial}{\partial r}\left(r\frac{\partial \in^{(n)}}{\partial r}\right) = 0, \tag{10}$$

$$\frac{1}{r}\frac{\partial}{\partial r}\left(r\frac{\partial u_r^{(n)}}{\partial r}\right) - \frac{u_r^{(n)}}{r^2} + \frac{1}{1-2\nu_n}\frac{\partial \in^{(n)}}{\partial r} = 0, \tag{11}$$

$$\in^{(n)} = \frac{1}{r}\frac{\partial\left(r u_r^{(n)}\right)}{\partial r}, \tag{12}$$

with $u_r^{(n)}$ as the non-zero displacement along the radial direction. The

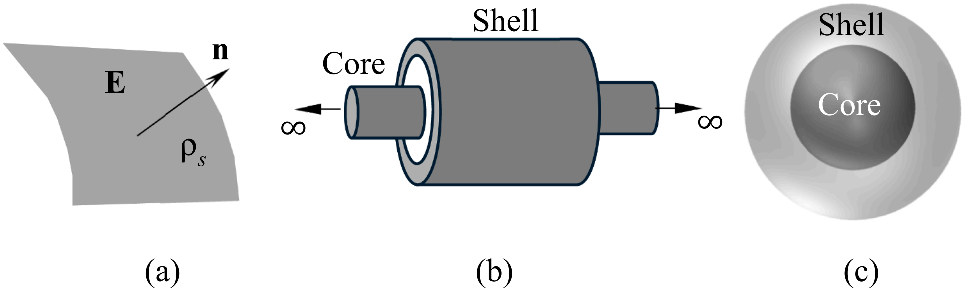

Fig. 1. Schematic of (a) electric field intensity, **E**, at the surface of a conducting material, (b) a cylindrical-shell structure, and (c) a spherical-shell structure.

general solutions of $\in^{(n)}$ and $u_r^{(n)}$ are

$$\in^{(n)} = A^{(n)} \text{ and } u_r^{(n)} = \frac{A^{(n)}}{2} r + \frac{B^{(n)}}{r}, \tag{13}$$

which gives the non-zero stress components of the stress tensor $\boldsymbol{\sigma}^{(n)}$ as

$$\sigma_{rr}^{(n)} = \frac{E_n}{(1+\nu_n)(1-2\nu_n)} \left[\frac{A^{(n)}}{2} - (1-2\nu_n) \frac{B^{(n)}}{r^2} \right], \tag{14}$$

$$\sigma_{\theta\theta}^{(n)} = \frac{E_n}{(1+\nu_n)(1-2\nu_n)} \left[\frac{A^{(n)}}{2} + (1-2\nu_n) \frac{B^{(n)}}{r^2} \right], \tag{15}$$

$$\sigma_{zz}^{(n)} = \frac{\nu_n E_n A^{(n)}}{(1+\nu_n)(1-2\nu_n)}. \tag{16}$$

Here, the superscript n takes the value of 1 or 2 with 1 representing the solid core and 2 representing the conducting shell. Using the boundary condition of (6) and $|\boldsymbol{\sigma}^{(1)}| < \infty$ as $r \to 0$, we obtain

$$\sigma_{rr}^{(1)} = \sigma_{\theta\theta}^{(1)} = \frac{1}{2\varepsilon_0} \left(\frac{Q}{2\pi a} \right)^2 \quad \text{for } r < a \tag{17}$$

$$\sigma_{zz}^{(1)} = \frac{\nu_1}{\varepsilon_0} \left(\frac{Q}{2\pi a} \right)^2 \quad \text{for } r < a \tag{18}$$

$$\sigma_{rr}^{(2)} = \frac{1}{2\varepsilon_0} \left(\frac{Q}{2\pi} \right)^2 \frac{1}{r^2} \quad \text{for } b \le r \le c, \tag{19}$$

$$\sigma_{\theta\theta}^{(2)} = -\frac{1}{2\varepsilon_0} \left(\frac{Q}{2\pi} \right)^2 \frac{1}{r^2} \text{ for } b \le r \le c, \tag{20}$$

$$\sigma_{zz}^{(2)} = 0 \quad \text{for } b \le r \le c. \tag{21}$$

It is interesting to note that the stress fields in both the cylindrical solid core and the cylindrical conducting shell are independent of Young's modulus of the corresponding materials. The cylindrical solid core experiences tensile stresses along the radial, axial and azimuth directions. In contrast, the cylindrical conducting shell experiences tensile stress along the radial direction and compressive stress along the azimuth direction. No axial stress is on the cylindrical conducting shell.

A spherical conducting solid core enclosed with a concentric spherical conducting shell

For the structure of a spherical conducting solid core of a in radius with a concentric spherical conducting shell of b ($b > a$) in inner radius and c in outer radius, the spherical solid core carries electric charge of Q, which induces opposite electric charge on the inner surface of the concentric spherical conducting shell and electric charge of the same sign on the outer surface of the concentric spherical conducting shell.

Provided that electric charges are uniformly distributed over individual surfaces, the charge densities on the surfaces of the spherical solid conductor and the spherical conducting shell can be expressed as

$$\rho_a = \frac{Q}{4\pi a^2}, \ \rho_b = -\frac{Q}{4\pi b^2} \text{ and } \rho_c = \frac{Q}{4\pi c^2} \tag{22}$$

for the surfaces with the radii of a, b, and c, respectively. Using Eq. (22), the electric field intensities on individual surfaces are found to be

$$\mathbf{E}_a = \frac{Q}{4\pi\varepsilon_0} \frac{1}{a^2} \mathbf{e}_r, \ \mathbf{E}_b = \frac{Q}{4\pi\varepsilon_0} \frac{1}{b^2} \mathbf{e}_r \text{ and } \mathbf{E}_c = \frac{Q}{4\pi\varepsilon_0} \frac{1}{c^2} \mathbf{e}_r \tag{23}$$

with $\mathbf{e}_r$ as the radial direction. The electric field acts on the electric charges in individual surfaces and introduces normal stress as

$$\sigma_n^{(a)} = \frac{1}{2\varepsilon_0} \left(\frac{Q}{4\pi a^2} \right)^2, \ \sigma_n^{(b)} = \frac{1}{2\varepsilon_0} \left(\frac{Q}{4\pi b^2} \right)^2 \text{ and } \sigma_n^{(c)} = \frac{1}{2\varepsilon_0} \left(\frac{Q}{4\pi c^2} \right)^2 \tag{24}$$

Here, all the surfaces are subjected to tensile normal stress.

With the characteristics of spherical symmetry, Eqs. (4)-(5) and the equation of $\in = \nabla \bullet \mathbf{u}$ are simplified as

$$\frac{1}{r^2} \frac{\partial}{\partial r} \left(r^2 \frac{\partial \in^{(n)}}{\partial r} \right) = 0, \tag{25}$$

$$\frac{1}{r^2} \frac{\partial}{\partial r} \left(r^2 \frac{\partial u_r^{(n)}}{\partial r} \right) - \frac{2u_r^{(n)}}{r^2} + \frac{1}{1-2\nu_n} \frac{\partial \in^{(n)}}{\partial r} = 0, \tag{26}$$

$$\in^{(n)} = \frac{1}{r^2} \frac{\partial \left(r^2 u_r^{(n)} \right)}{\partial r}, \tag{27}$$

with $u_r^{(n)}$ as the non-zero displacement along the radial direction. The general solutions of $\in^{(n)}$ and $u_r^{(n)}$ are

$$\in^{(n)} = A^{(n)} \text{ and } u_r^{(n)} = \frac{A^{(n)}}{3} r + \frac{B^{(n)}}{r^2}, \tag{28}$$

which gives the non-zero stress components of the stress tensor $\boldsymbol{\sigma}^{(n)}$ as

$$\sigma_{rr}^{(n)} = \frac{E_n}{(1+\nu_n)(1-2\nu_n)} \left[(1+\nu_n) \frac{A^{(n)}}{3} - 2(1-2\nu_n) \frac{B^{(n)}}{r^3} \right], \tag{29}$$

$$\sigma_{\theta\theta}^{(n)} = \frac{E_n}{(1+\nu_n)(1-2\nu_n)} \left[(1+\nu_n) \frac{A^{(n)}}{3} + (1-2\nu_n) \frac{B^{(n)}}{r^3} \right]. \tag{30}$$

Using the boundary conditions of (6) and $|\boldsymbol{\sigma}^{(1)}| < \infty$ as $r \to 0$, we obtain

$$\sigma_{rr}^{(1)} = \sigma_{\theta\theta}^{(1)} = \frac{1}{2\varepsilon_0} \left(\frac{Q}{4\pi a^2} \right)^2 \quad \text{for } r \le a, \tag{31}$$

$$\sigma_{rr}^{(n)} = -\frac{1}{2\varepsilon_0} \left(\frac{Q}{4\pi} \right)^2 \frac{1}{bc(c^3 - b^3)} \left((c-b) - \frac{c^4 - b^4}{r^3} \right) \quad \text{for } b \le r \le c, \tag{32}$$

$$\sigma_{\theta\theta}^{(n)} = -\frac{1}{2\varepsilon_0} \left(\frac{Q}{4\pi} \right)^2 \frac{1}{bc(c^3 - b^3)} \left((c-b) + \frac{1}{2} \frac{c^4 - b^4}{r^3} \right) \quad \text{for } b \le r \le c. \tag{33}$$

It is interesting to note that the stress fields in both the spherical solid core and the spherical conducting shell are independent of elastic constants of the corresponding materials. The spherical solid core experiences hydrostatic tensile stress. In contrast, the spherical conducting shell experiences tensile stress along the radial direction and compressive stress along the azimuth direction.

Numerical implementation

According to the above results, the stress field in the solid core is independent of spatial variable. The numerical calculation is thus focused on the radial and hoop stresses in the conducting shell. Fig. 2 shows spatial distribution of the radial and hoop stresses in a cylindrical conducting shell with $c/b = 2$. It is evident that the magnitudes of both the radial and hoop stresses decrease with the increase in the distance to the inner surface of the cylindrical conducting shell. The decrease of the radial stress with the increase in the distance to the inner surface of the cylindrical conducting shell can be associated with the requirement of force balance. From Eq. (9), the resultant force due to the electric stresses is zero along the radial direction for any arc-cylindrical section, indicating that the arc-cylindrical section is at equilibrium state under the action of the electric stresses.

Fig. 3 shows spatial distribution of the radial and hoop stresses in a spherical conducting shell with $c/b = 2$. Similar to the cylindrical conducting shell, the magnitudes of both the radial and hoop stresses decrease with the increase in the distance to the inner surface of the spherical conducting shell. The decrease of the radial stress with the

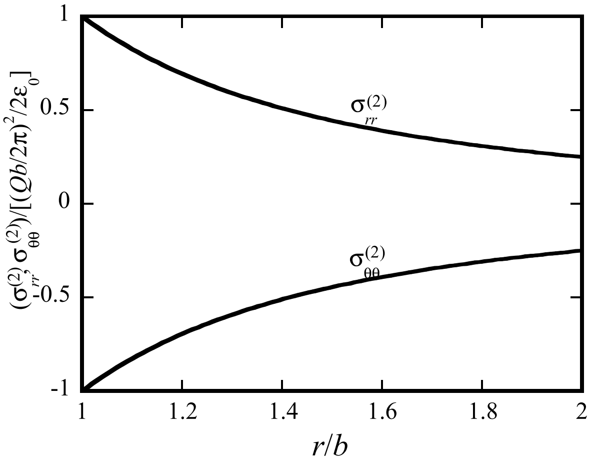

Fig. 2. Spatial variation of radial and hoop stresses in a cylindrical conducting shell ($c/b = 2$).

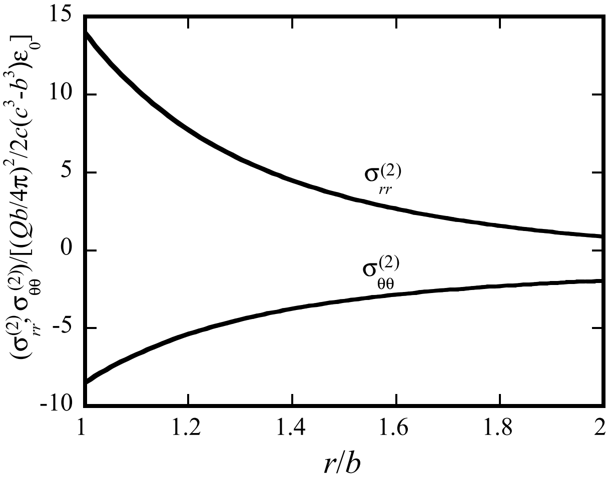

Fig. 3. Spatial variation of radial and hoop stresses in a spherical conducting shell ($c/b = 2$).

increase in the distance to the inner surface of the spherical conducting shell can be attributed to the decrease of the electric stress on the outer surface of the spherical conducting shell, which is inversely proportional to the fourth power of the radius of the outer surface.

Discussion

It is known that it is impossible to completely eliminate structural flaws, such as cracks and cavities, in a material. Electrical and/or mechanical stresses can cause growth of structural flaws, which can eventually lead to the failure and malfunction of associated structures and devices. From the above analysis, we note that both the solid conducting core and the hollow conducting shell experience tensile stress in the radial direction and the hollow conducting shell experiences compressive stress in the azimuth direction. Such stress distributions suggest that any cracks in the solid conducting core and the cracks with the crack plane near the crack edge/tip being normal to the radial direction in the hollow conducting shell can grow under the action of electric stresses when local tensile stress generated by the electric stresses reaches the critical stress for the formation and propagation of cracks. However, the compressive hoop stress hinders the formation and growth of cracks with the crack plane near the crack edge/tip normal to the azimuth direction in the hollow conducting shell.

Structural flaws formed during the forming and manufacturing generally exhibit the characteristics of randomness. Cracks with the crack plane near the crack edge/tip being parallel to axisymmetric axis for the cylindrical and spherical conducting shells, as shown in Fig. 4, can occur. Under such a configuration, it requires the determination of local stress state induced by electric stresses. For simplicity, we limit the following analysis to the total force on the S-section in the direction (**N**-direction) normal to the plane, which likely contains planar cracks.

Let λ be the distance between the plane and the axisymmetric axis (the center) of the cylindrical (spherical) conducting shell. For the cylindrical conducting shell, the resultant force per unit length, F_N, on the S-section in the **N**-direction is calculated as,

$$F_N = -\frac{1}{2\varepsilon_0}\left(\frac{Q}{2\pi b}\right)^2 \int_{-\theta}^{\theta} b\cos\alpha d\alpha + \frac{1}{2\varepsilon_0}\left(\frac{Q}{2\pi c}\right)^2 \int_{-\theta-\Delta\theta}^{\theta+\Delta\theta} c\cos\alpha d\alpha \tag{34}$$

$$= \frac{1}{\varepsilon_0}\left(\frac{Q}{2\pi}\right)^2 \left(\frac{\sin(\theta+\Delta\theta)}{c} - \frac{\sin\theta}{b}\right).$$

Here, the sinθ and sin(θ+Δθ) can be calculated from λ as

$$\sin\theta = \frac{\sqrt{b^2-\lambda^2}}{b} \text{ and } \sin(\theta+\Delta\theta) = \frac{\sqrt{c^2-\lambda^2}}{c}. \tag{35}$$

Substituting Eq. (35) in Eq. (34) yields

$$F_N = \frac{1}{\varepsilon_0}\left(\frac{Q}{2\pi}\right)^2 \left(\frac{\sqrt{c^2-\lambda^2}}{c^2} - \frac{\sqrt{b^2-\lambda^2}}{b^2}\right). \tag{36}$$

To have a repulsive force on the S-section, it requires $F_N > 0$. This gives

$$\lambda > \frac{bc}{(b^2+c^2)^{1/2}}. \tag{37}$$

The electric stresses introduce a resultant repulsive force on the S-section for λ satisfying Eq. (37), which can cause the formation and propagation of cracks in the planar faces of the S-section when local stresses generated by the electric stresses reach the critical stress.

For the spherical conducting shell, the resultant force, F_N, on the S-section in the **N**-direction is calculated as,

$$F_N = -\frac{1}{2\varepsilon_0}\left(\frac{Q}{4\pi b^2}\right)^2 \int_0^{\theta} 2\pi b^2 \sin\alpha\cos\alpha d\alpha + \frac{1}{2\varepsilon_0}\left(\frac{Q}{4\pi b^2}\right)^2 \int_0^{\theta+\Delta\theta} 2\pi c^2 \sin\alpha\cos\alpha d\alpha \tag{38}$$

$$= -\frac{1}{2\varepsilon_0}\left(\frac{Q}{4\pi}\right)^2 \left(\frac{\sin^2\theta}{b^2} - \frac{\sin^2(\theta+\Delta\theta)}{c^2}\right).$$

Here, the sinθ and sin(θ+Δθ) can be calculated from Eq. (35). Substituting Eq. (35) in Eq. (38) yields

$$F_N = \frac{1}{2\varepsilon_0}\left(\frac{Q}{4\pi}\right)^2 \left(\frac{c^2-\lambda^2}{c^4} - \frac{b^2-\lambda^2}{b^4}\right). \tag{39}$$

To have a repulsive force on the S-section, it requires $F_N > 0$. This gives

$$\lambda > \frac{bc}{(b^2+c^2)^{1/2}}. \tag{40}$$

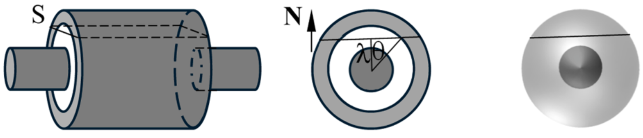

Fig. 4. Schematic of a plane parallel to axisymmetric axis.

which is the same as the case for the cylindrical conducting shell. The electric stresses introduce a resultant repulsive force on the S-section for λ satisfying Eq. (40), which can cause the formation and propagation of cracks in the planar faces of the S-section when local stresses generated by the electric stresses reach the critical stress.

Summary

In summary, we have brought out the important role of electric charge in the stress evolution of two physical configurations – the spherical core-shell and cylindrical core-shell structures. Using the theory of linear elasticity, both the stress and displacement fields have been obtained and proportional to the square of the charge carried by the solid conducting core. The spherical conducting core experiences hydrostatic tensile stress, and the cylindrical conducting core experiences tensile stress in the radial, axial and azimuth directions. Both the spherical and cylindrical conducting shells are subjected to tensile stress in the radial direction and compressive in the azimuth direction. There is no stress on the cylindrical conducting shell in the axial direction. The tensile stress in the radial direction can cause the formation and propagation of cracks with the crack plane near the crack edge/tip normal to the radial direction when local stress reaches the critical stress.

Using the electric stresses, we have calculated the resultant force on a section of the shell with the planar faces parallel to symmetrical axis for the spherical core-shell structure and the cylindrical core-shell structure. The direction of the resultant force is normal to the corresponding symmetrical axis. There exists a transition of the resultant force from attractive force to repulsive force. The presence of the repulsive force indicates that the electric stresses can also cause formation and propagation of cracks in the planar faces parallel to the corresponding symmetrical axis, leading to the failure and malfunction of associated structures and devices.

Understanding the mechanical deformation of core-shell structures in electric field allows for the determination of the critical field intensity for the occurrence of field-induced structural damage/degradation. The obtained result can be used to optimize the process parameters used in the field-assisted machining of tube-like structures to improve the structural integrity and in the production of core-shell structures of high quality for applications in metal-ion battery.

CRediT authorship contribution statement

Fuqian Yang: Writing – review & editing, Writing – original draft, Methodology, Investigation, Funding acquisition, Formal analysis, Data curation, Conceptualization.

Declaration of competing interest

The authors declare that they have no known competing financial interests or personal relationships that could have appeared to influence the work reported in this paper.

Acknowledgement

FY is grateful for the support by the NSF through the grant DMR-2409132 monitored by Dr. Jonathan D Madison and the grant CBET-2438033 monitored by Dr. Catherine Walker.

Data availability

Data will be made available on request.

References

[1] L. Bellaiche, A. García, D. Vanderbilt, Electric-field induced polarization paths in $Pb(Zr_{1-x}Ti_x)O_3$ alloys, Physical Review B 64 (2001) 060103.
[2] W. Ma, A. Hao, Electric field-induced polarization rotation and ultrahigh piezoelectricity in $PbTiO_3$, Journal of Applied Physics 115 (2014) 104105.
[3] R. Ignazzi, W.P. Gates, S.O. Diallo, D. Yu, F. Juranyi, F. Natali, H.N. Bordallo, Electric field induced polarization effects measured by in situ neutron spectroscopy, The Journal of Physical Chemistry C 121 (2017) 23582–23591.
[4] R.M. Martin, Piezoelectricity, Physical Review B 5 (1972) 1607–1613.
[5] W.P. Mason, Piezoelectricity, its history and applications, The journal of the Acoustical Society of America 70 (1981) 1561–1566.
[6] H. Kay, Electrostriction, Reports on Progress in Physics 18 (1955) 230–250.
[7] V. Sundar, R. Newnham, Electrostriction and polarization, Ferroelectrics 135 (1992) 431–446.
[8] R. Newnham, V. Sundar, R. Yimnirun, J. Su, Q. Zhang, Electrostriction: nonlinear electromechanical coupling in solid dielectrics, The Journal of Physical Chemistry B 101 (1997) 10141–10150.
[9] J. Grindlay, Electrostriction, Physical Review B 160 (1967) 698–701.
[10] A.I. Zhakin, Electrohydrodynamics, Physics-Uspekhi 55 (2012) 465–487.
[11] E.D. Fylladitakis, M.P. Theodoridis, A.X. Moronis, Review on the history, research, and applications of electrohydrodynamics, IEEE Transactions on Plasma Science 42 (2014) 358–375.
[12] P.M. Vlahovska, Electrohydrodynamics of drops and vesicles, Annual Review of Fluid Mechanics 51 (2019) 305–330.
[13] K. Iranshahi, T. Defraeye, R.M. Rossi, U.C. Müller, M. Transfer, Electrohydrodynamics and its applications: Recent advances and future perspectives, International Journal of Heat 232 (2024) 125895.
[14] L.D. Landau, E. Lifshitz, Electrodynamics of continuous media, 2nd ed., Elsevier, 1984.
[15] O. Hansen, J.T. Ravnkilde, U. Quaade, K. Stokbro, F. Grey, Field-induced deformation as a mechanism for scanning tunneling microscopy based nanofabrication, Physical Review Letters 81 (1998) 5572.
[16] F. Yang, W. Song, Morphological instability of elastic thin films-effect of electromechanical interaction, Applied Physics Letters 87 (2005) 111912.
[17] F. Yang, W. Song, Influence of electromechanical interaction on the morphological instability of an elastic conducting halfspace, Physical Review B 72 (2005) 165417.
[18] R. Huang, Electrically induced surface instability of a conductive thin film on a dielectric substrate, Applied Physics Letters 87 (2005) 151911.
[19] H. Li, L. Peng, B. Meng, Z. Xu, L. Wang, G. Ngaile, M. Fu, Manufacture, Energy field assisted metal forming: Current status, challenges and prospects, International Journal of Machine Tools & Manufacture 192 (2023) 104075.
[20] C. Tan, R. Li, J. Su, D. Du, Y. Du, B. Attard, Y. Chew, H. Zhang, E.J. Lavernia, Y. Fautrelle, Review on field assisted metal additive manufacturing, International Journal of Machine Tools & Manufacture 189 (2023) 104032.
[21] H.J. Biswal, J.J. Kaur, P.R. Vundavilli, A. Gupta, Recent advances in energy field assisted hybrid electrodeposition and electroforming processes, CIRP Journal of Manufacturing Science Technology 38 (2022) 518–546.
[22] J. Zhang, Z. Zheng, K. Huang, C. Lin, W. Huang, X. Chen, J. Xiao, J. Xu, Field-assisted machining of difficult-to-machine materials, International Journal of Extreme Manufacturing 6 (2024) 032002.
[23] D. Tian, T. Shi, X. Wang, H. Liu, X. Wang, Magnetic field-assisted acceleration of energy storage based on microencapsulation of phase change material with $CaCO_3/Fe_3O_4$ composite shell, Journal of Energy Storage 47 (2022) 103574.
[24] S. Ding, Y. Feng, X. Yue, Q. Zheng, Q. Hu, D. Lin, Electric-field-assisted alkaline hydrolysis of metal–organic framework bulk into highly porous hydroxide for energy storage and electrocatalysis, Inorganic Chemistry 61 (2022) 4948–4956.
[25] W. Wang, T. Yu, Y. Cheng, X. Lei, B. Wang, R. Guo, X. Liu, J. You, X. Wang, H. Zhang, Field-assisted metal-air batteries: recent progress, mechanisms, and challenges, Nano Energy 125 (2024) 109550.
[26] W. Wang, Y.C. Lu, External field-assisted batteries toward performance improvement, SusMat 3 (2023) 146–159.
[27] H. Conrad, Electroplasticity in metals and ceramics, Materials Science and Engineering: A 287 (2000) 276–287.
[28] N.K. Dimitrov, Y. Liu, M. Horstemeyer, Electroplasticity: A review of mechanisms in electro-mechanical coupling of ductile metals, Mechanics of Advanced Materials and Structures 29 (2022) 705–716.
[29] A. Lahiri, P. Shanthraj, F. Roters, Understanding the mechanisms of electroplasticity from a crystal plasticity perspective, Modelling and Simulation in Materials Science and Engineering 27 (2019) 085006.
[30] S. Zhao, R. Zhang, Y. Chong, X. Li, A. Abu-Odeh, E. Rothchild, D.C. Chrzan, M. Asta, J. Morris Jr, A.M. Minor, Defect reconfiguration in a Ti-Al alloy via electroplasticity, Nature materials 20 (2021) 468–472.
[31] G. Zhao, M. Liu, F. Yang, The effect of an electric current on the nanoindentation behavior of tin, Acta Materialia 60 (2012) 3773–3782.
[32] G. Zhao, F. Yang, Effect of DC current on tensile creep of pure tin, Materials Science and Engineering: A 591 (2014) 97–104.
[33] R. Chen, F. Yang, Effect of DC current on the creep deformation of tin, Journal of Electronic Materials 39 (2010) 2611–2617.
[34] G. Zhao, M. Liu, Z. An, Y. Ren, P.K. Liaw, F. Yang, Electromechanical responses of Cu strips, Journal of Applied Physics 113 (2013) 183521.
[35] G. Saulis, R. Rodaitė-Riševičienė, V. Snitka, Increase of the roughness of the stainless-steel anode surface due to the exposure to high-voltage electric pulses as revealed by atomic force microscopy, Bioelectrochemistry 70 (2007) 519–523.
[36] X. Wang, J. Guo, Y. Wang, X. Wu, B. Wang, Segregation of lead in Cu-Zn alloy under electric current pulses, Applied physics letters 89 (2006).
[37] J. Liu, R. Niu, J. Gu, M. Cabral, M. Song, X.J.S.r. Liao, Effect of ion irradiation introduced by focused ion-beam milling on the mechanical behaviour of sub-micron-sized samples, 10 (2020) 10324.

[38] J. Li, A.K. Dozier, Y. Li, F. Yang, Y.-T. Cheng, Crack pattern formation in thin film lithium-ion battery electrodes, Journal of The Electrochemical Society 158 (2011) A689.

[39] F. Shi, Z. Song, P.N. Ross, G.A. Somorjai, R.O. Ritchie, K. Komvopoulos, Failure mechanisms of single-crystal silicon electrodes in lithium-ion batteries, Nature Communications 7 (2016) 11886.

[40] W. An, P. He, Z. Che, C. Xiao, E. Guo, C. Pang, X. He, J. Ren, G. Yuan, N.J.A.A.M. Du, Interfaces, Scalable synthesis of pore-rich Si/C@C core–shell-structured microspheres for practical long-life lithium-ion battery anodes, 14 (2022) 10308-10318.

[41] Z. Liu, S. Jin, K. Cui, J. Zhao, S. Xie, J. Li, C.J.J.o.A. Xinghua, Compounds, Cavity containing core-shell Bi@C nanowires toward high performance lithium ion batteries, 842 (2020) 155796.

[42] P. Hou, H. Zhang, Z. Zi, L. Zhang, X. Xu, Core-shell and concentration-gradient cathodes prepared via co-precipitation reaction for advanced lithium-ion batteries, Journal of Materials Chemistry A 5 (2017) 4254–4279.

[43] L.-F. Cui, Y. Yang, C.-M. Hsu, Y. Cui, Carbon-silicon core-shell nanowires as high capacity electrode for lithium ion batteries, Nano Letters 9 (2009) 3370–3374.

[44] G. Tan, F. Wu, Y. Yuan, R. Chen, T. Zhao, Y. Yao, J. Qian, J. Liu, Y. Ye, R. Shahbazian-Yassar, Freestanding three-dimensional core–shell nanoarrays for lithium-ion battery anodes, Nature Communications 7 (2016) 1–10.